Journal of Materiomics 6 (2020) 248–255

Contents lists available at ScienceDirect

Journal of Materiomics

journal homepage: www.journals.elsevier.com/journal-of-materiomics/

Thermal studies of individual Si/Ge heterojunctions — The influence of the alloy layer on the heterojunction

Sien Wang [a, 1], Dongchao Xu [a, 1], Ramya Gurunathan [b], G. Jeffrey Snyder [b], Qing Hao [a, *]

[a] Department of Aerospace and Mechanical Engineering, University of Arizona, Tucson, AZ, 85721-0119, USA
[b] Department of Materials Science and Engineering, Northwestern University, Evanston, IL, 60208, USA

ARTICLE INFO

Article history:
Received 10 December 2019
Received in revised form
12 February 2020
Accepted 29 February 2020
Available online 2 March 2020

Keywords:
Thermal boundary resistance
Si/Ge heterojunction
Film-wafer bonding
Phonon

ABSTRACT

Phonon transport across an interface is of fundamental importance to applications ranging from electronic and optical devices to thermoelectric materials. The phonon scattering by an interface can dramatically suppress the thermal transport, which can benefit thermoelectric applications but create problems for the thermal management of electronic/optical devices. In this aspect, existing molecular dynamics simulations on phonon transport across various interfaces are often based on estimates of atomic structures and are seldom compared with measurements on real interfaces. In this work, planar Si/Ge heterojunctions formed by film-wafer bonding are measured for the interfacial thermal resistance (R_K) that is further compared with predictions from existing simulations and analytical models. The twist angle between a 70-nm-thick Si film and a Ge wafer is varied to check the influence of the crystal misorientation. Detailed transmission electron microscopy studies are carried out to better understand the interfacial atomic structure. It is found that the alloyed interfacial layer with mixed Si and Ge atoms dominates the measured thermal resistance (R_K). Some oxygen impurities may also help to increase R_K due to the formation of glassy structures. Following this, R_K reduction should be focused on how to minimize the interdiffusion of Si and Ge atoms during the formation of a Si/Ge heterojunction.

1. Introduction

For many engineering applications, phonon transport across an interface has remained as one central topic for research on nanoscale heat transfer [1,2]. In physics, the phonon reflection and transmission by an interface can introduce an interfacial thermal resistance R_K, known as the Kapitza resistance [3–5]. However, the exact interaction between an interface and incident phonons is still not well understood even after decades of research. In the widely used acoustic mismatch model (AMM) and diffuse mismatch model (DMM), an interface is viewed as a plane joining two materials and the bulk phonon properties of both materials are used to compute the phonon transmissivity τ and thus R_K. The atomic structure and intrinsic properties of the interface are not considered though a real interface can be a complicated layer region with disorder, roughness, dislocation arrays, and often atom intermixing [6]. In the extended DMM, an interfacial layer is viewed as a third medium with unique properties, which is sandwiched between two sides of an interface [7]. Recently, the mixed mismatch model (MMM) was proposed by taking partially specular and partially diffuse transmission into account [8]. It can better predict the interfacial thermal resistance with an arbitrary surface roughness. In more advanced studies, the interactions between a phonon and an interface can be extracted from molecular dynamics (MD) simulations [9–12] and the atomistic Green's function (AGF) approach [13–16]. By merging lattice dynamics methods with MD simulations, a new formalism termed interface conductance modal analysis was also used to study interfacial phonon transport [17]. However, the assumed interfacial structures are usually oversimplified and direct comparison to measurements are mostly restricted to high-quality interfaces associated with thin films grown or deposited on a substrate [18–21]. In contrast, more defects are usually found on the nanosized interfaces within a material synthesized by hot pressing nanopowder into the bulk form. Particularly for heterojunctions, interdiffusion of different atoms during the high-temperature material synthesis can introduce an alloy layer to largely restrict the phonon transport. The alloy

* Corresponding author.
E-mail address: qinghao@email.arizona.edu (Q. Hao).
Peer review under responsibility of The Chinese Ceramic Society.
[1] The two authors contribute equally to this paper.

https://doi.org/10.1016/j.jmat.2020.02.013

interfacial layer was neglected in many molecular dynamics studies on Si/Ge heterojunctions [12,22,23] but was incorporated in one recent study [16], in which the alloy layer was found to significantly suppress the interfacial phonon transport. An increase in alloy layer thickness was predicted to strongly reduce both the phonon transmissivity and the effect of lattice mismatch.

Experimentally, it is still challenging to measure a single interface within a bulk material. As a simpler approach, bonding between two rigid wafers has been used to represent a twist grain boundary for thermal studies [24,25]. However, the interfacial thermal stress introduced during the bonding process can largely affect the quality of the formed interface, which becomes more critical for two different materials such as Si and Ge. This problem can be solved by bonding a super-flexible thin film onto a rigid wafer. In this case, the thermal-mismatch strain energy is almost entirely stored inside the film and the total stored energy is proportional to the small film thickness. The flexible thin film also ensures good adhesion between the film and rigid wafer to ensure good contact for bonding formation. Extremely high-quality bonding has been demonstrated between a 200-nm-thick and millimeter-sized Si membrane and a Ge wafer, with thin ~1.2 nm region for the bonded Si–Ge interface as revealed by cross-sectional transmission electron microscopy (TEM) studies [26].

In this work, the high-quality bonded interface between a 70-nm-thick (100) Si film and a (100) Ge wafer was used to study the formation and the resulting R_K for the corresponding heterojunction. Different twist angles between the Si film and the Ge wafer were used to check the impact of misorientations on R_K. The experimental data were directly compared to existing simulations. Systematic TEM studies were carried out to better understand the complicated interfacial atomic structure, particularly the SiGe alloy layer at the interface. The studied Si/Ge heterojunctions were widely used in high-performance photodiodes [27,28], thermoelectric nanocomposites [29,30], superlattice nanowires and thin films [31,32]. Unrestricted to Si/Ge interfaces, R_K studies of film-wafer bonding are critical to many applications that use film-wafer bonding for microdevice fabrication and thermal management of power devices, e.g., GaN-diamond bonding for better heat dissipation [33].

2. Experimental

2.1. Film-wafer bonding

The employed 70-nm-thick Si film was released as the device layer from a commercial silicon-on-insulator (SOI) wafer. Strips with the width of 400 μm were defined using photolithography. The unprotected part of the Si thin film was etched using reactive ion etch while the thin film to be transferred was under protection of the photoresist. The Si film was released from the SOI wafer by etching off the buried SiO_2 layer on a SOI wafer with hydrofluoric acid (HF). With the photoresist as the protection layer, the film transfer process was similar to those widely used for two-dimensional materials [34]. As an alternative way, a thermal release tape may also be used for the film transfer process [26]. The photoresist or residue from the thermal release tape was removed with acetone and then isopropyl alcohol (IPA). On the other side, the Ge substrates were cleaned by sonication in acetone, IPA and deionized (DI) water for 15 min each. The Ge substrate was further cleaned with HF:HCl:H_2O (1:1:10) solution for 20 min [26]. HF should leave an oxygen free surface and HCl should leave a carbon free surface. In the final step, Ge substrates were rinsed under DI water for 10 min to remove the HF/HCl residue on the Ge surface.

The Si/Ge bonding was formed by annealing the samples at 673 K for 30 min in a tube furnace with nitrogen flow, following the previous work on Si/Ge bonding [26]. The temperature was ramped up slowly at the rate of 5 K/min to minimize any damages due to the mismatch between the thermal expansion coefficients of Si and Ge. The same 5 K/min rate was used during the cool down process. Fig. 1a shows the scanning electron microscopy (SEM) image of a 70-nm-thick Si film bonded onto a Ge substrate. Using an atomic force microscope (AFM), the surface undulation across the Si film was mostly <1 nm over a 5 μm × 5 μm region after thermal bonding (Fig. 1b).

In the standard synthesis of bulk SiGe nanocomposites, a pressure is applied during the hot press process [35,36]. However, it was found that adding a moderate ~50 MPa pressure during the bonding process may cause wrinkles on the relatively soft Ge substrate. Therefore, thermal bonding for typical device fabrications was employed here and no pressure was applied.

2.2. Thermal characterization

For measurements, an 80-nm-thick Al_2O_3 layer was deposited across the whole wafer for electrical insulation. On the Ge substrate, the region without the bonded Si film was used as the reference. For measured regions, 20-nm-thick Cr and then 200-nm-thick Au were deposited as a metal-line heater/thermometer (Fig. 2 inset). The metal line was 20 μm wide and 3.5 mm long, ensuring one-dimensional heat conduction through the 70 nm film thickness.

An offset 3ω technique [37,38] was used to measure the summation of the cross-plane thermal resistances for the Si film (R_{Film}) and the Si/Ge interfacial R_K. The difference in the R_K values for the Al_2O_3/Si and Al_2O_3/Ge interfaces is neglected in the data analysis. In existing measurements, the R_K of an Al_2O_3/Si interface is 6.92 ± 0.50 m^2 K/GW at 300 K [39]. Although there is no reported R_K value for an Al_2O_3/Ge interface, this value is anticipated to be close to that for an Al_2O_3/Si interface because Ge and Si both have a similarly large ~30% lattice mismatch with deposited Al_2O_3, using a lattice constant of 7.91 Å for the Al_2O_3 layer [40]. The difference between these two R_K values is negligible compared with the measured R_K for a Si/Ge interface, which is above 28 m^2 K/GW at all temperatures (Fig. 7a). In comparison measurements, $R_{Film} + R_K$ can be extracted from the in-phase AC temperature oscillation ΔT_{AC} curves for a film-wafer assembly compared to a reference location on the same Ge wafer (Fig. 2). In the linear regime, these two ΔT_{AC} curves are shifted by a constant value, $P(R_{Film} + R_K)/A$. Here P and A are the amplitude of the heating power at the 2ω frequency and area of the metal line, respectively.

Detailed uncertainty analysis of similar film-wafer measurements can be found in our previous work [41]. For the metal line with its electrical resistance R_{Metal}, the uncertainty of its temperature coefficient of resistance (TCR) is negligible in the 3ω measurement. In this aspect, the associated slope dR_{Metal}/dT is mainly affected by the ~0.01 K repeatability of thermocouple reading, instead of the 1–2 K system error (offset) of the temperature reading. As one example, accurate Seebeck coefficients can be measured based on the slope $d\Delta V/d\Delta T$ for varied voltage difference ΔV and temperature difference ΔT applied across a sample, where the maximum ΔT can be only ~1 K [42].

In data analysis, $R_{Film} + R_K$ is extracted by averaging the $\Delta T_{AC}A/P$ shift over all frequencies in Fig. 2. For this averaged $R_{Film} + R_K$, the half width of its 95% confidence interval (u_R) ranges from 1.8×10^{-10} to 2.4×10^{-9} m^2 K/W for all temperature-dependent measurements, which is within 2.4% of the extracted $R_{Film} + R_K$ value. The second error source can be the thickness variation of the deposited Al_2O_3 layer on the film-wafer assembly and at the reference location on the same Ge wafer. This thickness variation was within 0.5 nm, as checked with spectroscopic reflectometry (Filmetrics F-20). In the literature, the cross-plane thermal conductivity of a similar Al_2O_3

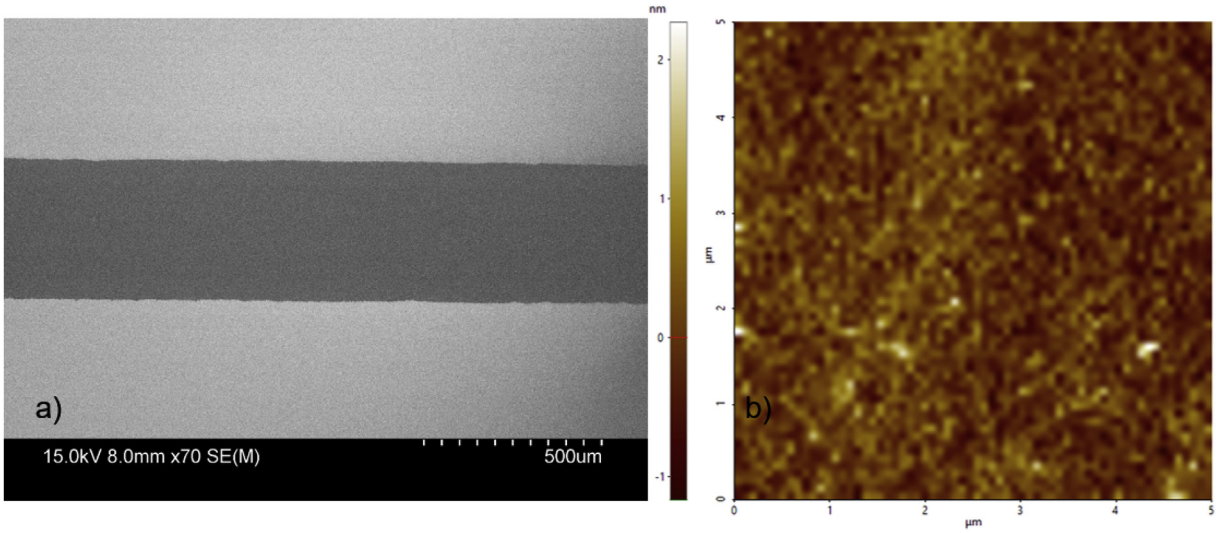

Fig. 1. (a) SEM image of a Si film on a Ge wafer. (b) Surface undulation of a Si film bonded onto a Ge substrate.

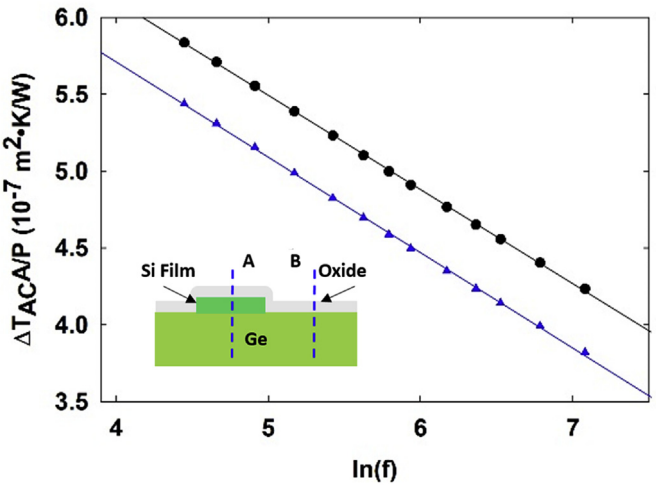

Fig. 2. $\Delta T_{AC}A/P$ for an offset 3ω test, with the inset showing the cross-section diagram of the measurement setup. Usually 13 frequencies are selected for each sample (symbols) and the linear fitting of the data shows $R^2 > 0.9998$. The black curve and circles are for location A, with Al_2O_3-coated film-wafer assembly. The blue curve and triangles are for reference location B, without the Si film. The shift between the two curves is $R_{Film} + R_K$ per unit area.

layer was measured at different temperatures [43]. Computed as the layer thickness divided by the cross-plane thermal conductivity, the cross-plane thermal resistance per unit area for the Al_2O_3 layer thus has an uncertainty $u_{Al_2O_3}$ decreasing from 8.3×10^{-10} m^2 K/W at 77 K to 3.1×10^{-10} m^2 K/W at 300 K. The overall uncertainty is computed as $\sqrt{u_R^2 + u_{Al_2O_3}^2}$ for extracted $R_{Film} + R_K$.

3. Results and discussion

3.1. Cross-plane R_{Film} calculation

Because the offset 3ω technique cannot separate R_{Film} and R_K, the required cross-plane R_{Film} is calculated using the film thickness $t = 70$ nm and bulk phonon MFP $\Lambda_{\mathrm{Bulk},\,i}(\omega)$, the latter of which depends on the phonon branch i and phonon angular frequency ω. The effective phonon MFP, $\Lambda_{\mathrm{eff},\,i}(\omega)$, is expressed as $1/\Lambda_{\mathrm{eff},\,i}(\omega) = 1/\Lambda_{\mathrm{Bulk},\,i}(\omega) + 4/3t$ [44]. This effective phonon MFP is then input into the kinetic relationship, i.e., $k_L = \frac{1}{3}\sum_{i=1}^{3}\int_0^{\omega_{max,i}} C_i(\omega)v_{g,i}(\omega)\Lambda_{\mathrm{eff},\,i}(\omega)d\omega$, where C is the spectral heat capacity per unit volume and v_g is the phonon group velocity. At 300 K, the bulk phonon MFPs computed in Esfarjani et al. were utilized [45]. Below 300 K, the temperature dependence of $\Lambda_{\mathrm{Bulk},\,i}(\omega)$ was taken into account by a scaling factor $g(T) = T[1 - \exp(-3T/\Theta_D)]$, i.e. $\Lambda_{\mathrm{Bulk},\,i}(\omega,T) \sim \frac{1}{g(T)}$, using a Debye temperature of $\Theta_D = 645$ K [46]. The details of this calculation can be found in our previous work [41]. The computed cross-plane k_L is plotted in Fig. 3, in comparison to the room-temperature value calculated by Jeong et al. [47] that employs the exact phonon dispersion and fitted phonon MFPs. The thermal resistance of the thin film is further calculated with $R_{Film} = t/k_L$. This R_{Film} is less than 8% of the extracted R_K at 300 K and decreases to 1.5% of the extracted R_K at 83 K.

3.2. TEM studies of the interfacial atomic structure

Fig. 4a and b show the interfacial atomic structures of two

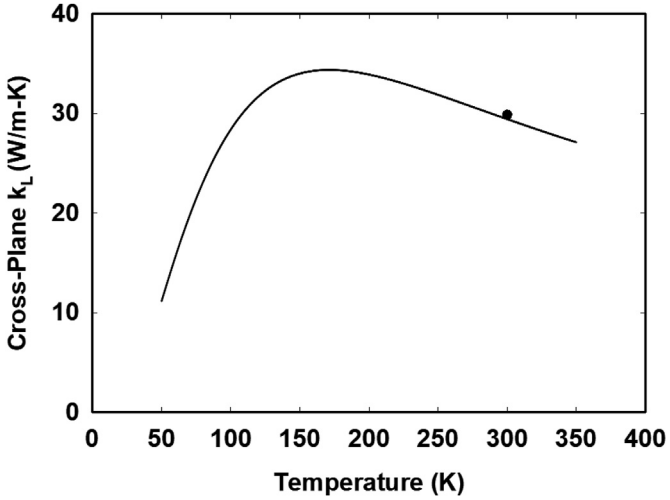

Fig. 3. Temperature-dependent cross-plane k_L computed for a 70-nm-thick Si film. The black dot is based on the calculation by Jeong et al. [47].

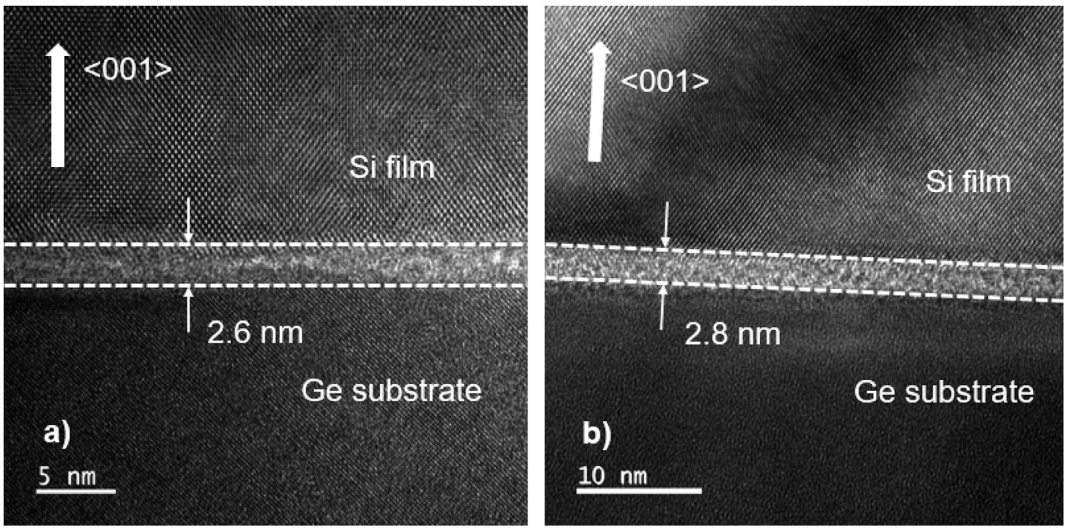

Fig. 4. Cross-sectional TEM images of film-wafer interfaces with a twist angle of (a) 1.1° and (b) 12.6°. The interface region is enclosed by dashed lines, with the thickness indicated.

representative samples with twist angles of 1.1° and 12.6° between the Si film and Ge wafer, respectively. For TEM studies, both samples are cut from the film-wafer assembly with a focused ion beam (FIB) and then transferred onto a TEM grid. An interfacial layer (or interlayer) of around 2.6–2.8 nm thickness can be observed at the Si/Ge interface. The sample with a 12.6° twist angle has a slightly thicker interface. The observed interlayer thickness is comparable to the ~2 nm thickness for bonding formed between a Si wafer and a Ge wafer below 673 K [28], and the ~3 nm thickness for room-temperature bonding between Si and Ge ribbons [48]. Additional 673 K annealing for 30 min in N_2 can increase the interlayer thickness to 3.5 nm for ribbon bonding [48]. A slightly thinner ~1.2 nm interlayer has also been observed for the bonding between a Si film and a Ge wafer at 673 K in previous work [26]. The divergence between various studies can be attributed to the slightly stronger/weaker surface oxidation on the Ge wafer before the thermal bonding [48,49].

Plane-view TEM image (Fig. 5) of the sample with a 1.1° twist angle is also taken at the interface. A periodic atomic structure with mixed Si and Ge atoms can be found. In our previous work on Si/Si bonding [41], an array of dislocations can be found at the film-wafer bonded interface. When the dislocation array exists, the distance between adjacent dislocations should be [50]

$$S_d = \frac{a_1 a_2}{\sqrt{2(a_1^2 + a_2^2 - 2a_1 a_2 cos\theta)}} \quad (1)$$

in which a_1 and a_2 are the lattice constants for the two crystals, θ is the twist angle between the two crystals. For Si and Ge, $S_d = 8.7$ nm is predicted with Eq. (1) and such a large S_d is not observed here. The interfacial alloy region formed by Si/Ge interdiffusion may largely affect the dislocations predicted by the model in Eq. (1).

Energy-dispersive X-ray spectroscopy (EDS) is conducted to further study the elemental composition across the interface. Similar results have been observed for the two samples with 1.1° and 12.6° twist angles so that only the 12.6° sample is presented here. The element mapping (Fig. 6a) reveals that the interface region mainly consists of Si, Ge and O. An almost uniform C percentage of around 2%–3% is observed for the whole cross section, which can be attributed to the C contamination within the FIB chamber. Excess C contamination has been reported at the Si/Ge interface [48,51] and has been suspected to be the result of the residue from the thermal release tape [48]. However, C contamination at the interface is not found in the current study, in which a thermal release tape is not used. Other than Si and Ge, the higher O concentration at the interface is mostly due to the immediate oxidation of a Ge wafer in the air, even after the HF treatment [48,49]. When the Si film is in contact with Ge, the Ge–O bonds can be replaced by Si–O bonds even at room temperature [52]. More bond replacement can be triggered by high temperature annealing and the O peak location can be moved toward the Si side. Different from Si/Ge bonding with certain interface oxidation, an almost uniform O distribution across the whole cross section and thus no remarkable interface oxidation have been found in similar studies for Si/Si bonding when both the Si film and its bonded Si wafer are passivated with HF cleaning [41].

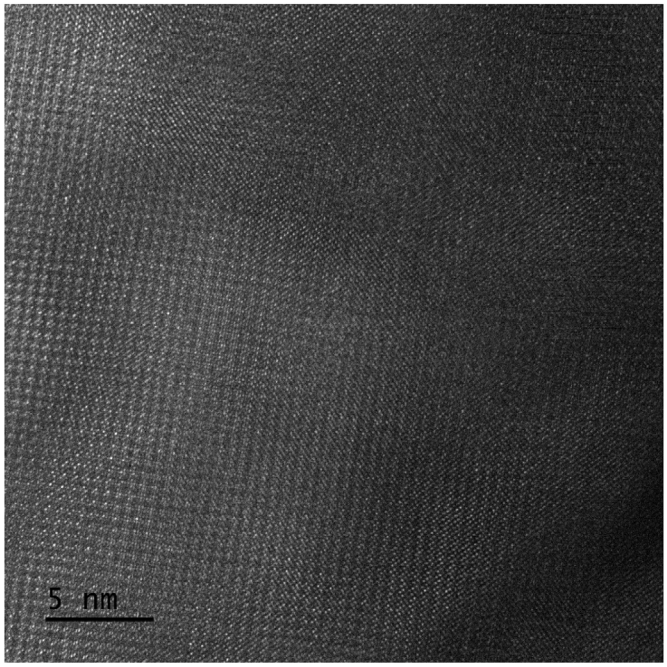

Fig. 5. Plane-view TEM image for a Si/Ge interface with a 1.1° twist angle.

Along the scanning direction indicated in Fig. 6b, the EDS line

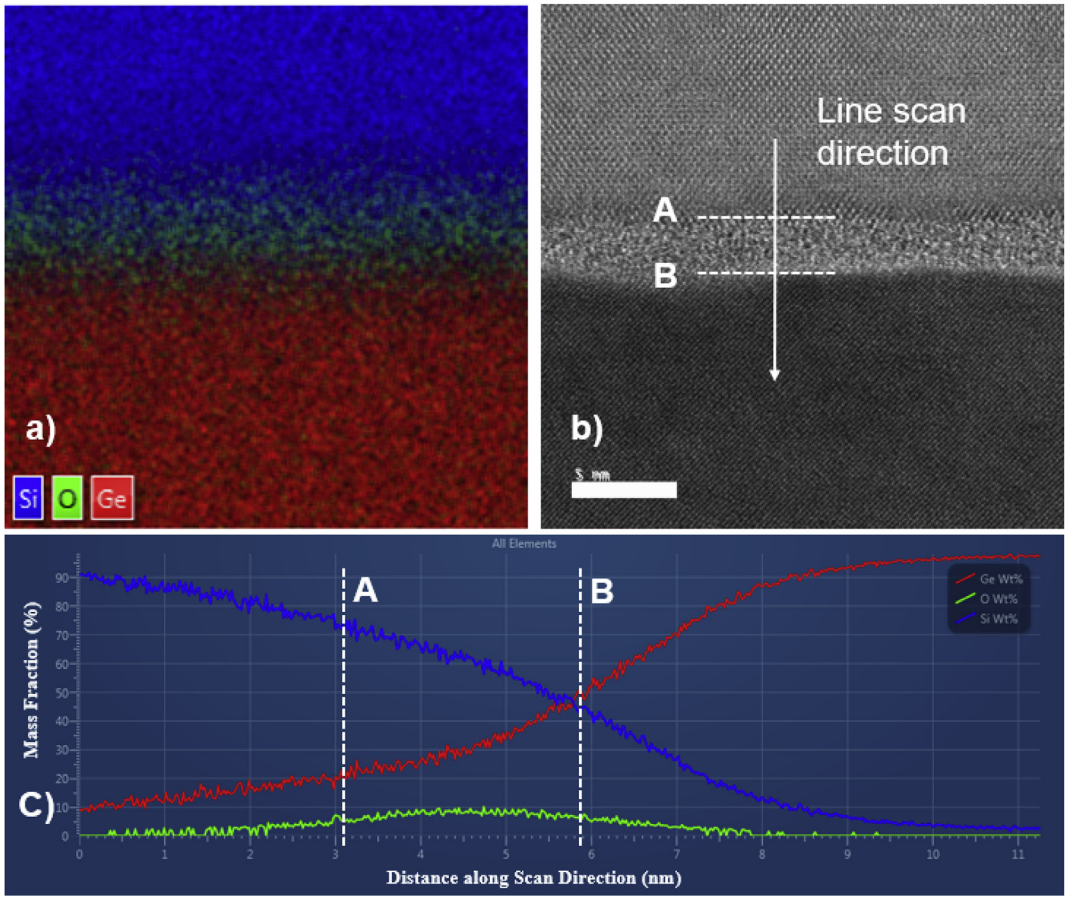

Fig. 6. (a) Element mapping of the Si/Ge interface for the sample with a 12.6° twist angle. (b) SEM image of the element mapping area. (c) EDS line scan across the interface, along the A–B direction indicated by (b).

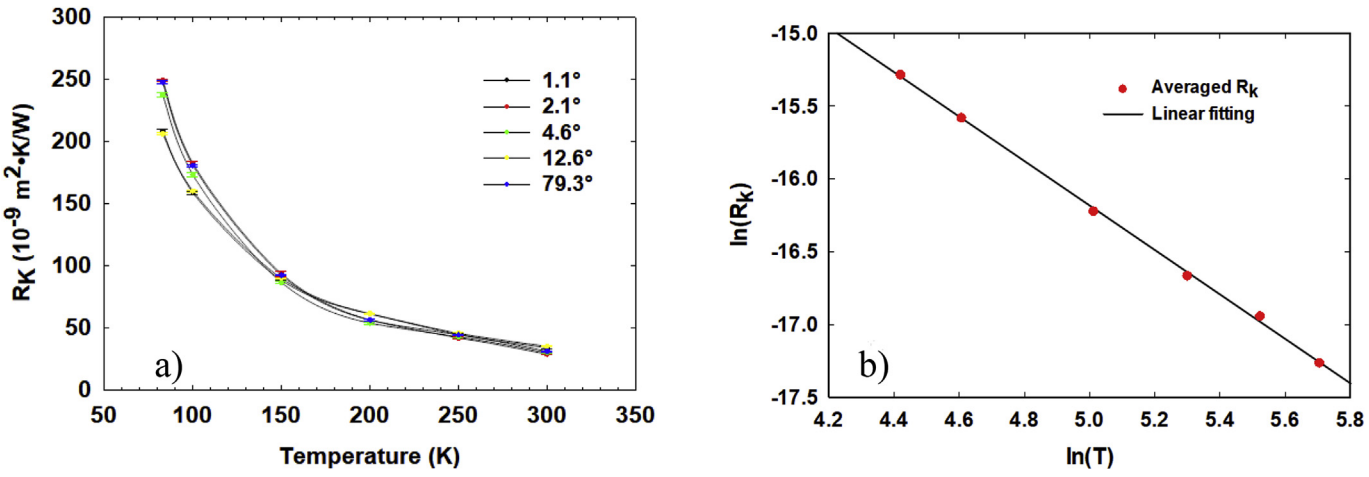

Fig. 7. (a) Temperature-dependent R_K for representative samples with different twist angles. (b) log-log plot showing the power law relationship of averaged $R_K \propto T^{-1.5}$.

scan (Fig. 6c) shows the element distribution across the interface. The interdiffusion of Si and Ge atoms can be found even outside the interface region that is indicated by the A-B section. The Si/Ge interface is suggested to be a layer of mixed SiO_x and Ge [48]. In such cases, the O concentration at the interface and interlayer thickness can be critical to the thermal transport across the interface. In analogy, electrical measurements across such junctions shows a dramatically reduced on-current when the interlayer thickness is increased from 3 nm to 3.5 nm after 673 K annealing [48]. For thermal transport, reducing the interfacial R_K requires minimized Ge surface oxidation during the fabrication process.

3.3. Temperature-dependent R_K of Si/Ge heterojunctions with varied twist angles

Fig. 7a shows the extracted interfacial R_K for Si/Ge bonding, with

the error bars indicating the uncertainty $\sqrt{u_R^2 + u_{Al_2O_3}^2}$ described in Section 2.2. The measured R_K showed a weak dependence on the twist angle between the film and the wafer. A temperature dependence of $R_K \sim T^{-1.5}$ is determined for the whole temperature range, which is below the Debye temperature (Θ_D) of both Si and Ge (Fig. 7b). In this regime, the temperature dependence is mainly determined by Bose-Einstein statistics, and R_K is predicted to eventually plateau at $T > \Theta_D$[4,5].

In comparison, film-wafer bonding studies for an Si/Si interface show strong twist angle dependence for the interfacial R_K, which is further correlated with periodic strain fields at the interface [41]. In analyzing the power law dependence on temperature, the n exponent in the $R_K \sim T^{-n}$ relation also depends on the twist angle for the Si/Si interface, where n ranges from 0.7 to 0.9 for a bonded Si/Si interface [41]. This temperature dependence has been explained by a frequency-dependent scattering of phonons at the interface that emerges from the interface's underlying periodic structure [53,54]. In the measured Si/Ge interface, however, n appears to be independent of twist angle. The SiGe alloy layer is amorphous and has no long-range order. Therefore, the phonon transport across the boundary has little dependence on the misorientation angle. In this situation, the R_K should be more sensitive to the element composition across a Si/Ge interface. Our EDS study indicates that the element composition is almost identical for the 1.1° and 12.6° samples. This could be explained by the same annealing condition for both samples. It also suggests that the interdiffusion of Si and Ge atoms has very weak dependence on the twist angle. General discussions on R_K are given for two surfaces bridged by an intermediate layer [55], i.e., a SiGe alloy layer for Si/Ge interfaces measured in this work.

In comparison, the computed or measured room-temperature R_K values of similar interfaces are listed in Table 1. The measured R_K values for Si/Ge bonding here are generally higher than those for Si/Si bonding, the latter of which ranges from 5.5×10^{-9} m^2 K/W to 2.8×10^{-8} m^2 K/W at 300 K [41]. The contrast here suggests the dominant effects of the amorphous interlayer for blocking the thermal transport. Without considering any oxidation, molecular dynamics simulations suggest that the SiGe alloy interlayer functions as the major bottleneck for the interfacial thermal transport [16]. For an interlayer thickness of 2.27 nm, R_K of ~1.0×10^{-8} m^2 K/W at 300 K is computed for Si/Ge bonding with a 0° twist angle. The higher R_K values measured in this work are attributed to the slightly thicker interlayer and amorphous SiO_x within the interlayer. In addition, the interdiffusion between Si and Ge extends beyond the <3 nm interlayer in Fig. 6c. These additional alloy regions are also resistive to thermal transport.

4. Conclusions

In conclusion, systematic thermal studies have been carried out on the bonded interfaces between a 70-nm-thick (100) Si film and a (100) Ge substrate, which can represent similar heterojunctions formed within SiGe thermoelectric nanocomposites [29,30] and devices fabricated using film-wafer bonding [27,28]. In particular, the twist angle between the film and wafer is varied to check the impact of the crystal misorientation on the resulting interfacial thermal resistance R_K. It has been found that R_K has a weak dependence on the twist angle and is generally much higher than the predicted R_K on the order of 1×10^{-9}m^2·K/W for an ideal Si/Ge interface [12,22,23], i.e., without defects or an interfacial alloy layer due to the interdiffusion of Si and Ge atoms. In contrast, a similar study on Si/Si bonding indicates a strong twist-angle dependence of R_K, along with a much lower R_K value [41]. Our measured high R_K for an Si/Ge interface is mainly attributed to the <3 nm thick alloy layer and some oxidation on the interface, as suggested by one previous molecular dynamics study [16]. The interdiffusion across the interface can be further found within an ~10 nm region around the interface. In addition, the temperature dependence is well aligned with the $R_K \sim T^{-1.5}$ power law. Future studies should consider the special lattice vibration modes within the interfacial layer [17] and the complicated defects across an interface [6]. In practice, controlling the thickness of the interfacial layer with optimized bonding conditions can also be used as an effective approach to tailor the R_K value.

Table 1
Comparison of measured or computed R_K for Si/Ge and other interfaces at 300 K.

Interface Type	Method	R_K(m^2·K/GW)
Si/Ge	Experiment	28.8–35.1(This work)
Si/Ge	DMM	3.7 [22]
Si/Ge	MD	3.0–3.9 [22]
Si/Ge	MD	3.2 [12]
Si/Si	Experiment	5.5–29.0 [41]
Si/SiO_2	Experiment	21.3 [56]
SiC/SiO_2	Experiment	80.8 [56]

Declaration of competing interest

The authors declare that they have no known competing financial interests or personal relationships that could have appeared to influence the work reported in this paper.

Acknowledgements

Qing Hao thanks the support from National Science Foundation CAREER Award (grant number CBET-1651840). TEM and SEM analyses were performed at the Kuiper Materials Imaging and Characterization facility and we gratefully acknowledge NASA (grants #NNX12AL47G and #NNX15AJ22G) and NSF (grant #1531243) for funding of the instrumentation in the Kuiper Materials Imaging and Characterization Facility at the University of Arizona. The authors also thank TEM manager Jerry Chang for his assistance. RG and GJS thank U.S. Department of Commerce, National Institute of Standards and Technology as part of the Center for Hierarchical Materials Design (CHiMaD) grant 70NANB19H005.

References

[1] Cahill DG, Braun PV, Chen G, Clarke DR, Fan S, Goodson KE, Keblinski P, King WP, Mahan GD, Majumdar A, Maris HJ, Phillpot SR, Pop E, Shi L. "Nanoscale thermal transport. II. 2003–2012. Appl Phys Rev 2014;1(1):011305.
[2] Cahill DG, Ford WK, Goodson KE, Mahan GD, Majumdar A, Maris HJ, Merlin R, Phillpot SR. Nanoscale thermal transport. J Appl Phys 2003;93(2):793–818.
[3] Kapitza PL. The study of heat transfer in helium II. J Phys 1941;4:181.
[4] Swartz ET, Pohl RO. Thermal boundary resistance. Rev Mod Phys 1989;61(3):605–68.
[5] Monachon C, Weber L, Dames C. Thermal boundary conductance: a materials science perspective. Annu Rev Mater Res 2016;46:433–63.
[6] Hopkins PE. Thermal transport across solid interfaces with nanoscale imperfections: effects of roughness, disorder, dislocations, and bonding on thermal boundary conductance. ISRN Mech Eng 2013:682586. 2013.
[7] Beechem T, Graham S, Hopkins P, Norris P. Role of interface disorder on thermal boundary conductance using a virtual crystal approach. Appl Phys Lett 2007;90(5):054104.
[8] Zhang Y, Ma D, Zang Y, Wang X, Yang N. A modified theoretical model to accurately account for interfacial roughness in predicting the interfacial thermal conductance. Front Energy Res 2018-June;6(48). 2018.
[9] Maiti A, Mahan G, Pantelides S. "Dynamical simulations of nonequilibrium processes—heat flow and the Kapitza resistance across grain boundaries. Solid State Commun 1997;102(7):517–21.
[10] Stevens RJ, Zhigilei LV, Norris PM. "Effects of temperature and disorder on thermal boundary conductance at solid–solid interfaces: nonequilibrium molecular dynamics simulations. Int J Heat Mass Tran 2007;50(19–20):3977–89.

[11] Kimmer C, Aubry S, Skye A, Schelling PK. Scattering of phonons from a high-energy grain boundary in silicon: dependence on angle of incidence. Phys Rev B 2007;75(14):144105.
[12] Landry E, McGaughey A. Thermal boundary resistance predictions from molecular dynamics simulations and theoretical calculations. Phys Rev B 2009;80(16):165304.
[13] Sadasivam S, Che Y, Huang Z, Chen L, Kumar S, Fisher TS. "The atomistic Green's function method for interfacial phonon transport. Ann. Rev. Heat Transfer 2014;17:89–145.
[14] Zhang W, Fisher T, Mingo N. Simulation of interfacial phonon transport in Si–Ge heterostructures using an atomistic Green's function method. J Heat Tran 2007;129(4):483–91.
[15] Zhang W, Fisher T, Mingo N. The atomistic Green's function method: an efficient simulation approach for nanoscale phonon transport. Numer Heat Tran, Part B: Fundamentals 2007;51(4):333–49.
[16] Li X, Yang R. Effect of lattice mismatch on phonon transmission and interface thermal conductance across dissimilar material interfaces. Phys Rev B 2012;86(5):054305.
[17] Gordiz K, Henry A. Phonon transport at crystalline Si/Ge interfaces: the role of interfacial modes of vibration. Sci Rep 2016;6:23139.
[18] Costescu RM, Wall MA, Cahill DG. Thermal conductance of epitaxial interfaces. Phys Rev B 2003;67(5):054302.
[19] Sarua A, Ji H, Hilton K, Wallis D, Uren MJ, Martin T, Kuball M. Thermal boundary resistance between GaN and substrate in AlGaN/GaN electronic devices. IEEE Trans Electron Dev 2007;54(12):3152–8.
[20] Hopkins PE, Duda JC, Clark SP, Hains CP, Rotter TJ, Phinney LM, Balakrishnan G. Effect of dislocation density on thermal boundary conductance across GaSb/GaAs interfaces. Appl Phys Lett 2011;98(16):161913.
[21] Kim EK, Kwun SI, Lee SM, Seo H, Yoon JG. Thermal boundary resistance at $Ge_2Sb_2Te_5$/ZnS:SiO_2 interface. Appl Phys Lett 2000;76(26):3864–6.
[22] Zhan T, Minamoto S, Xu Y, Tanaka Y, Kagawa Y. Thermal boundary resistance at Si/Ge interfaces by molecular dynamics simulation. AIP Adv 2015;5(4):047102.
[23] Chalopin Y, Esfarjani K, Henry A, Volz S, Chen G. Thermal interface conductance in Si/Ge superlattices by equilibrium molecular dynamics. Phys Rev B 2012;85(19):195302.
[24] Tai K, Lawrence A, Harmer MP, Dillon SJ. Misorientation dependence of Al_2O_3 grain boundary thermal resistance. Appl Phys Lett 2013;102(3):034101.
[25] Hurley DH, Khafizov M, Shinde S. Measurement of the Kapitza resistance across a bicrystal interface. J Appl Phys 2011;109(8):083504.
[26] Kiefer AM, Paskiewicz DM, Clausen AM, Buchwald WR, Soref RA, Lagally MG. Si/Ge junctions formed by nanomembrane bonding. ACS Nano 2011;5(2):1179–89.
[27] Tseng C-K, Chen W-T, Chen K-H, Liu H-D, Kang Y, Na N, Lee M-CM. A self-assembled microbonded germanium/silicon heterojunction photodiode for 25 Gb/s high-speed optical interconnects. Sci Rep 2013;3:3225.
[28] Kanbe H, Miyaji M, Ito T. Ge/Si heterojunction photodiodes fabricated by low temperature wafer bonding. APEX 2008;1(7):072301.
[29] Jeng M-S, Yang R, Song D, Chen G. Modeling the thermal conductivity and phonon transport in nanoparticle composites using Monte Carlo simulation. J Heat Tran 2008;130(4):042410.
[30] Hao Q, Zhao H, Xiao Y, Xu D. Thermal investigation of nanostructured bulk thermoelectric materials with hierarchical structures: an effective medium approach. J Appl Phys 2018;123(1):014303.
[31] Lin K-H, Strachan A. Thermal transport in SiGe superlattice thin films and nanowires: effects of specimen and periodic lengths. Phys Rev B 2013;87(11).115302, 03/04/.
[32] Hu M, Poulikakos D. Si/Ge superlattice nanowires with ultralow thermal conductivity. Nano Lett 2012;12(11):5487–94. 2012/11/14.
[33] Cho J, Li Z, Bozorg-Grayeli E, Kodama T, Francis D, Ejeckam F, Faili F, Asheghi M, Goodson KE. "Improved thermal interfaces of GaN–diamond composite substrates for HEMT applications. IEEE Trans Compon Packag Manuf Technol 2013;3(1):79–85.
[34] Chen Y, Gong XL, Gai JG. Progress and challenges in transfer of large-area graphene films. Adv Sci 2016;3(8).
[35] Zhou J, Li X, Chen G, Yang R. Semiclassical model for thermoelectric transport in nanocomposites. Phys Rev B 2010;82(11):115308.
[36] Minnich A, Dresselhaus M, Ren Z, Chen G. Bulk nanostructured thermoelectric materials: current research and future prospects. Energy Environ Sci 2009;2(5):466–79.
[37] Cahill DG. Thermal conductivity measurement from 30 to 750 K: the 3 omega method. Rev Sci Instrum 1990;61(2):802–8.
[38] Cahill DG, Katiyar M, Abelson JR. Thermal conductivity of a-Si:H thin films. Phys Rev B 1994;50(9):6077–81.
[39] Scott EA, Gaskins JT, King SW, Hopkins PE. Thermal conductivity and thermal boundary resistance of atomic layer deposited high-k dielectric aluminum oxide, hafnium oxide, and titanium oxide thin films on silicon. Apl Mater 2018;6(5):058302.
[40] Wu SY, Hong M, Kortan AR, Kwo J, Mannaerts JP, Lee WC, Huang YL. High-quality thin single-crystal γ-Al2O3 films grown on Si (111). Appl Phys Lett 2005;87(9):091908.
[41] Xu D, Hanus R, Xiao Y, Wang S, Snyder GJ, Hao Q. Thermal boundary resistance correlated with strain energy in individual Si film-wafer twist boundaries. Mater Today Phys 2018;6:53–9.
[42] de Boor J, Müller E. Data analysis for Seebeck coefficient measurements. Rev Sci Instrum 2013;84(6):065102.
[43] Cahill DG, Lee SM, Selinder TI. Thermal conductivity of κ-Al2O3 and α-Al2O3 wear-resistant coatings. J Appl Phys 1998;83(11):5783–6. 1998/06/01.
[44] Majumdar A. Microscale heat conduction in dielectric thin films. J Heat Tran 1993;115(1):7–16.
[45] Esfarjani K, Chen G, Stokes HT. Heat transport in silicon from first-principles calculations. Phys Rev B 2011;84(8):085204. 08/23/.
[46] Ward A, Broido D. Intrinsic phonon relaxation times from first-principles studies of the thermal conductivities of Si and Ge. Phys Rev B 2010;81(8):085205.
[47] Jeong C, Datta S, Lundstrom M. Thermal conductivity of bulk and thin-film silicon: a Landauer approach. J Appl Phys 2012;111(9):093708.
[48] Liu TC, Kabuyanagi S, Nishimura T, Yajima T, Toriumi A. n+Si/pGe heterojunctions fabricated by low temperature ribbon bonding with passivating interlayer. IEEE Electron Device Lett 2017;38(6):716–9.
[49] Park K, Lee Y, Lee J, Lim S. Oxidation mechanism of hydrogen-terminated Ge (100) surface. Appl Surf Sci 2008;254(15):4828–32.
[50] Sagalowicz L, Rudra A, Syrbu A, Behrend J. Structure of the wafer fused InP (001)-GaAs (001) interface. Phil Mag Lett 1997;76(6):445–52.
[51] Kanbe H, Hirose M, Ito T, Taniwaki M. Crystallographic properties of Ge/Si heterojunctions fabricated by wet wafer bonding. J Electron Mater 2010;39(8):1248–55.
[52] Prabhakaran K, Matsumoto T, Ogino T, Masumoto Y. Fabrication of multi-period Si/SiO 2/Ge layered structure through chemical bond manipulation. Appl Phys Lett 1998;72(24):3169–71.
[53] Wang Z, Alaniz JE, Jang W, Garay JE, Dames C. Thermal conductivity of nanocrystalline silicon: importance of grain size and frequency-dependent mean free paths. Nano Lett 2011;11(6):2206–13. 2011/06/08.
[54] Hao Q. "General effective medium formulation for thermal analysis of a polycrystal—the influence of partially specular phonon transmission across grain boundaries. J Appl Phys 2014;116(3):034305.
[55] Polanco CA, Rastgarkafshgarkolaei R, Zhang J, Le NQ, Norris PM, Ghosh AW. Design rules for interfacial thermal conductance: building better bridges. Phys Rev B 2017;95(19):195303.
[56] Deng S, Xiao C, Yuan J, Ma D, Li J, Yang N, He H. Thermal boundary resistance measurement and analysis across SiC/SiO2 interface. Appl Phys Lett 2019;115(10):101603.

Sien Wang is a Ph.D. student of Department of Aerospace and Mechanical Engineering at the University of Arizona. He received his B.S degree from Shanghai Jiao Tong University, China in 2017. His research interests include characterization of thermal and electrical properties of nanostructured thin films and 2D materials.

Dongchao Xu is a Ph.D. graduate student in Mechanical Engineering from University of Arizona. He received B.S. degree in Mechanical Engineering from Zhejiang University, China, in 2010. His research interests focus on thermoelectric studies of nanoporous thin films and 2D materials.

R. Gurunathan is currently a Ph.D. student in the Department of Materials Science and Engineering at Northwestern University under the direction of Prof. G. Jeffrey Snyder. She received her B.S. in Materials Science and Engineering from Penn State University as well as an MPhil in Scientific Computing from the University of Cambridge through the Churchill Scholarship. Her research interests include using analytical, physics-based models to understand thermal transport in materials with crystalline defects.

G. Jeffrey Snyder is a Professor of Materials Science and Engineering at Northwestern University. His interest is focused on thermoelectric engineering and advanced materials development such as complex Zintl phase and nanostructured bulk thermoelectric materials (http://thermoelectrics.matsci.northwestern.edu/). He has over 400 publications in thermoelectrics that are highly cited (Thomson Reuters 2016-8) and mentored several students and postdocs in the field including three Goldsmid and two ITS Young Investigator Award winners.

Qing Hao is an Associate Professor of Department of Aerospace and Mechanical Engineering at the University of Arizona. His research focuses on nanoscale energy transport in materials and electronic devices, including thermoelectrics, high-power electronics, and 2D materials. He received the 2008 R&D 100 Award as a team member for thermoelectrics research, 2015 AFOSR YIP Award for graphene studies, and 2017 NSF CAREER Award for thermal studies of grain boundaries.